Environmental Science Nano

Elemental fingerprint as a potential tool for tracking the fate of real-life model nanoplastics generated from plastic consumer products in environmental systems

Journal:	*Environmental Science: Nano*
Manuscript ID	EN-ART-08-2023-000559.R1
Article Type:	Paper

Environmental Significance

One of the current pressing challenges in investigating the fate of nanoplastics in living organisms and environmental systems is the inability to track nanoplastics in environmental and biological media. Recent efforts have focused on synthesizing metal-doped nanoplastics to achieve this purpose. However, only a limited number of metal-doped nanoplastics have been synthesized so far, which tend to lack the true representation of real-life nanoplastics. This study quantified the elemental concentration and fingerprint in real-life nanoplastics derived from plastic consumer products and environmentally aged plastic fragments using state-of-the-art analytical methods. This study provides a tool, based on elemental fingerprints, to track the fate of real-life model nanoplastics in controlled laboratory studies. It expands the realm of nanoplastics that can be followed based on their metallic signatures to all kinds of plastics. Additionally, this study illustrates the importance of nanoplastics as a source of metals and metal-bearing nanoparticles in the environment.

Elemental fingerprint as a potential tool for tracking the fate of real-life model nanoplastics generated from plastic consumer products in environmental systems

Mohammed Baalousha[1]*, Jingjing Wang[1], Md Mahmudun Nabi[1], Mahbub Alam[1], Mahdi Erfani[2], Julien Gigault[3], Florent Blancho[4], Mélanie Davranche[4], Phillip Potter[5], Souhail R. Al-Abed[5]

Affiliations:

[1] Center for Environmental Nanoscience and Risk, Department of Environmental Health Sciences, Arnold School of Public Health, University of South Carolina, SC 29208, United States

[2] Department of Civil and Environmental Engineering, University of South Carolina, SC 29208, USA

[3] TAKUVIK Laboratory, CNRS/Université Laval, 1045, av. de La Médecine, Québec G1V 0A6, Canada

[4] Géosciences Rennes, CNRS/Université de Rennes, 263 av. Général Leclerc, 35000 Rennes, France

[5] Office of Research and Development, Center for Environmental Solutions and Emergency Response, US Environmental Protection Agency, 26 W. Martin Luther King Drive, Cincinnati, OH 45268, United States

* Corresponding author: mbaalous@mailbox.sc.edu

Abstract

Metals and metalloids are widely used in producing plastic materials as fillers and pigments, which can be used to track the environmental fate of real-life nanoplastics in environmental and biological systems. Therefore, this study investigated the metal and metalloids concentrations and fingerprint in real-life model nanoplastics generated from new plastic products (NPP) and from environmentally aged ocean plastic fragments (NPO) using single particle-inductively coupled plasma-mass spectrometry (SP-ICP-TOF-MS) and transmission electron microscopy coupled with energy dispersive x-ray spectroscopy (TEM-EDX). The new plastic products include polypropylene straws (PPS), polyethylene terephthalate bottles (PETEB), white low-density polyethylene bags (LDPEB), and polystyrene foam shipping material (PSF). All real-life model nanoplastics contained metal and metalloids, including Si, Al, Sr, Ti, Fe, Ba, Cu, Pb, Zn, Cd, and Cr, and were depleted in rare earth elements. Nanoplastics generated from the white LDPEB were rich in Ti-bearing particles, whereas those generated from PSF were rich in Cr, Ti, and Pb. The Ti/Fe in the LDPEB nanoplastics and the Cr/Fe in the PSF nanoplastics were higher than the corresponding ratios in natural soil nanoparticles (NNPs). The Si/Al ratio in the PSF nanoplastics was higher than in the NNPs, possibly due to silica-based fillers. The elemental ratio of Si/Al, Fe/Cr, and Fe/Ni in the nanoplastics derived from ocean plastic fragments was intermediate between the nanoplastics derived from real-life plastic products and NNPs, indicating a combined contribution from pigments and fillers used in plastics and from natural sources. This study provides a method to track real-life nanoplastics in controlled laboratory studies based on nanoplastic elemental fingerprints. It expands the realm of nanoplastics that can be followed based on their metallic signatures to all kinds of nanoplastics. Additionally, this study illustrates the importance of nanoplastics as a source of metals and metal-containing nanoparticles in the environment.

1. Introduction

Plastic pollution is a serious global environmental problem and receives considerable attention from government agencies, research communities, and the general public [1-3]. The global production of plastics exceeds 250-300 million metric tons per year and is expected to double in the next two decades [4-6]. Due to improper disposal and transport via wind and surface runoff, large quantities of plastics enter environmental systems. These plastics break down in the environment into increasingly smaller particles down to the nano-size range (*i.e.,* nanoplastics, 1-100 or 1-1000 nm [7, 8]), known as secondary (or real-life) nanoplastics [6, 9]. Consequently, plastic particles of various sizes, shapes, and polymeric compositions are widely distributed in the environment and found in freshwater [10, 11] and marine ecosystems [12, 13], fish [14], birds [15], and even in the Arctic and Antarctic sea ice [16]. Thus, there is an increased global interest in understanding the environmental fate and effects of the different classes of plastic particles, including nanoplastics. So far, many studies have investigated the occurrence and characteristics of plastic fragments and microplastics in environmental [10, 17-19] and biological systems [14, 15]. Fewer studies investigated the fate and effects of mainly synthetic (*e.g.,* commercially available) microplastics (*e.g.,* polystyrene, polypropylene, polyethylene, polyvinyl chloride) [20-22] and even fewer studies investigated the fate and effects of synthetic nanoplastics, typically polystyrene [20-22]. This is because synthetic microplastics of different polymer types are commercially available, but polystyrene nanoplastics are the only commercially available nanoplastics [20-25].

Moreover, several research groups synthesized metal-labeled nanoplastics (*e.g.,* palladium-doped polystyrene spheres [26] and indium-doped polyester fibers [27], heteroaggregation of positively charged gold nanoparticle with negatively charged nanoplastics [28, 29]) to track nanoplastics in environmental and biological media using the metal signature [26]. Therefore, the current knowledge on the environmental fate and effects of nanoplastics is limited to a few types of nanoplastics due to the lack of synthetic nanoplastics of different polymer types, sizes, and shapes. Such knowledge also might not represent the

true environmental fate and effects of real-life nanoplastics, which cover a broad spectrum of polymers, sizes, shapes, and additives.

Real-life nanoplastics are different from synthetic nanoplastics in many essential aspects. **1)** Real-life nanoplastics contain constituents not present in synthetic nanoplastics, such as pigments and fillers [30, 31], which influence the environmental fate and adverse effects of nanoplastics. These additives could impact the environmental fate and effects of real-life nanoplastics compared to synthetic nanoplastics. **2)** Real-life nanoplastics occur in various shapes, sizes, and colors. However, synthetic nanoplastics are typically available only in smooth spheres [26-29]. **3)** Synthetic nanoplastics surfaces are often modified/functionalized to maximize colloidal dispersion of otherwise hydrophobic nanoplastics [26]. For instance, polystyrene latex beads contain high concentrations of surfactants (*e.g.,* sodium dodecyl sulfate (SDS) [32], but the composition and concentration of the surfactants are often not included in ingredient labels. Such information is proprietary and is typically not disclosed by manufacturers, which hampers assessing their impact on the environmental fate and adverse effects of synthetic nanoplastics. These surfactants are well known to influence nanoplastics aggregation, settling, biological uptake, and toxicity. **4)** Commercial nanoplastics are often formulated with a biocide to prevent bacterial growth during delivery and storage. Additionally, synthetic nanoplastics may contain other ingredients not disclosed by the manufacturers.

Inorganic additives may account for up to 60 wt.% of plastic composition [33]. Typical fillers include SiO_2, $BaSO_4$, TiO_2, clays, talc ($MgSi_4O_{10}(OH)_2$), and kaolinite ($Al_2Si_2O_5(OH)$). Inorganic pigments include various metal oxides, such as iron, titanium, chromium, cadmium, and lead oxides [34]. These fillers and pigments have been detected in various types of plastics. For instance, food packaging plastics have been shown to contain nickel, cadmium, cobalt, copper, lead, chromium, zinc, and iron [35]. Drinking water bottles have been shown to contain antimony, lead, cadmium, and other metals [36, 37]. Analysis of nanoplastics by scanning electron microscopy coupled with energy-dispersive X-ray spectroscopy (SEM-EDX) illustrates the presence of Si, Al, Fe, Zn, S, Ba, Br, and Ti in marine plastics [38, 39]; Si, Al, Mg, and Fe in microplastics

used in exfoliating products [40]; and Al, Si, Na, and Nb in microplastics found in Malaysian commercial fish [41]. However, little attention has been given to the impact of inorganic additives in determining the environmental risks of nanoplastics. These metal additives could be used as tracers to track the environmental fates of real-life nanoplastics, thereby opening a window toward investigating all types of polymers, sizes, and shapes of real-life nanoplastics.

Single particle-inductively coupled plasma-mass spectrometry (SP-ICP-MS) is a powerful tool for particle quantification [42]. It has been commonly used for the detection and quantification of metal(loid)s-bearing nanoparticles or cells [43, 44]. Additionally, it has been recently used for the detection of carbon in microplastics [45-49]. The size detection limit of metal(loid)s-bearing nanoparticles varies from few to several hundreds of nanometers [50] whereas that of carbon-bearing particles (microplastics) varies from 0.62 to 1.8 µm [45-47], depending on instrument sensitivity, target element, and media composition. Additionally, single particle-inductively coupled plasma-time of a flight-mass spectrometry (SP-ICP-TOF-MS) has been recently used for the simultaneous detection of carbon and rare earth elements (REEs) in synthetic REE-doped polystyrene microplastics [47]. However, SP-ICP-TOF-MS has never been implemented to measure elemental fingerprints in nanoplastics generated from consumer products or from ocean plastic fragments.

This study characterizes the elemental (metals and metalloids) fingerprint in model real-life nanoplastics generated from new plastic products (NPP) used in our daily lives and from environmentally aged ocean plastic fragments (NPO). The elemental fingerprint in the nanoplastics was compared to those in natural nanoparticles (NNPs) extracted from three soil samples to identify unique elemental signatures in model real-life nanoplastics. The elemental fingerprints within nanoplastics were determined using ICP-TOF-MS in conventional and single particle analysis modes to cross validate the results using bulk elemental ratios and single particle elemental ratios. The multi-element single particles events were classified into clusters of events of similar elemental composition using a two-stage agglomerative

hierarchical clustering analysis approach to reduce the large data produced by SP-ICP-TOF-MS into a reportable format.

2. Materials and Methods

2.1. Generation of nanoplastics from plastic consumer products

Model real-life nanoplastics were generated from consumer products (NPP) using a kitchen blender. Plastic products were chosen based on polymer and product type. The most common polymers in environmental plastic samples are polypropylene, polyethylene terephthalate, polyethylene, and polystyrene [5]. A typical consumer product for each polymer type was selected: polypropylene drinking straw (PPS), polyethylene terephthalate soda bottle (PETEB), white low-density polyethylene shopping bag (LDPEB), and polystyrene (PSF) foam packing material. The plastic consumer products were cut into small (~1 cm) pieces. They were placed in approximately 500 mL of SuperQ water in a 1 L beaker and broken down using a commercially available kitchen-style stick blender. The blender was rinsed extensively with SuperQ water before and between plastic sample blending to avoid cross contamination. SuperQ water without plastic products was blended similarly as a procedural blank. The blender was operated by hand and used in 5 sequential 30 s intervals separated by 60 s breaks to prevent overheating of the blender motor. Plastic samples and SuperQ water without plastics products were filtered through a 0.45 μm Whatman syringe filter to remove particles outside the nanomaterial size range. Dynamic light scattering (DLS) measurements were acquired using a Malvern Zetasizer to confirm the presence/absence of newly formed nanoplastics and the SuperQ water in the blended samples. Preliminary experiments analyzed with DLS showed no particle formation from the blender in Super Q water. The polydispersity of the generated nanoplastics prevented accurate determination of their z-average hydrodynamic diameter, but the higher signal response compared to SuperQ water allowed the qualitative confirmation of the formation of nanoplastics.

2.2. Generation and characterization of nanoplastics from ocean fragments (NPO)

Environmentally aged ocean plastic fragments were collected from the North Pacific garbage patch (provided by Ocean-Clean-Up NGO). Four different batches of plastic debris were selected to generate nanoplastics. The plastic debris were selected based on their degree of weathering/oxidation state because the formation of nanoplastics increases with the degree of weathering [27]. Model real-life Nanoplastics (labeled Nanoplastics 1, 2, 3, and 4) were generated from the environmentally aged ocean plastic fragments according to the previously established protocol [51]. Briefly, the ocean plastic fragments were mixed with deionized (DI) water at a 1:2 plastic:DI ratio (w/w) in a square bottle and stirred at 250 rpm for 48 h, followed by sonication for 1 h, then filtration at 40 µm cut-off cellulose acetate filter (VWR, Radnor, PA, USA). The resulting particles were treated with H_2O_2/UV for 5 h to remove associated organic matter and algal residue. Then, the nanoplastics size fraction was separated by filtration over a 1.2 µm cut-off glass fiber filter (Prat DUMAS, Couze-et-Saint-Front, France). The H_2O_2 was removed by diafiltration using a 20 kDa PES membrane (Microdyn-Nadir, Goleta, CA, USA). The hydrodynamic diameter of the nanoplastics was determined using Dynamic Light Scattering (DLS) (VASCO Flex's, Cordouan Technologies, Pessac, France). The morphology of the nanoplastics was examined by transmission electron microscopy (TEM, JEM 2100 HR, Jeol, Tokyo, Japan). The TEM samples were prepared by depositing 2.5 µL of the nanoplastics suspension on a carbon-coated grid (Oxford instrument, Abingdon, UK). The TEM was operated at 200-kV acceleration voltage with a LaB_6 as an electron source with a point and line resolution of 2.3 Å and 1.4 Å, respectively. Particles were photographed with a Gatan Orius SC200D camera, and elemental analyses were performed using an EDX Oxford X-Max 80T detector. The polymer composition of the nanoplastics was determined using Fourier-transform-infra red spectroscopy (FT-IR) and Pyrolysis-Gas Chromatography-Mass Spectrometry (Py-GCMS, Pyrolyzer PY-3030 Frontier Lab, GC, and MS from Agilent Technologies mass spectrometer, 5977B, Santa Clara, CA, USA) according to the method described elsewhere [51]. Pyrolysates were separated using Helium as carrier gas on a C18 capillary column (DB5, 30m

for Polyethylene and 60m for Polypropylene and natural organic matter, Agilent Technologies). Pyrolysates were identified by comparing the PyGCMS mass spectra of the environmentally aged plastics with the National Institute of Standards and Technology (NIST) database for eluted peaks and the F-Search database to determine the polymeric composition of the nanoplastics (FrontierLab, Japan).

2.3. Soil samples

Three topsoil samples, Orangeburg, Varina, and Mecklenburg, were collected with a hand drill from the surface to 15 cm below the surface in polyethylene bags described elsewhere [52]. The Orangeburg soil was collected from Dillon County (34.5044, -79.4231452), the Varina soil was collected from Dillon County (34.455574, -79.444813), and the Mecklenburg soil was collected from Chester County (34.80189, -80.07951139), South Carolina, United States. Natural nanoparticles were extracted from the soils as described elsewhere [52]. Briefly, the soils were sieved using a 10-mesh 2 mm pore-size nylon sieve (Zhangxing Instrument, Shanghai, China). A hundred grams of the dry-sieved soils were mixed with 1 L ultrapure water (UPW, Millipore Advantage System, Merck Millipore, Darmstadt, Germany) for 24 h, followed by wet sieve through a 300-mesh 54 μm pore size nylon sieve (Zhangxing Instrument, Shanghai, China). Then, the sieved soil samples were freeze-dried (Labconco FreeZone 6 Liter, Kansas City, MO, USA). Twenty mg of the freeze-dried soils were mixed with 30 mL UPW in 50 mL acid-washed polypropylene centrifuge tubes and overhead rotated on a tube rotator at 40 rpm (Fisher Scientific, Shanghai, China) overnight. The well-dispersed mixture was bath sonicated (Branson 2800, 40 kHz, Dandury, CT, USA) for 2 h to disrupt soil microaggregates and enhance the dispersion of NNPs [53]. The 1 μm size fraction was then separated by centrifugation (Eppendorf, 5810 R, Hamburg, Germany) at 775 g for 5 min based on a 2.5 $g \cdot cm^{-3}$ particle density and Stokes' law calculation [54]. The top 20 mL of the supernatant was transferred into 50 mL acid-washed polypropylene centrifuge tubes and stored at 4 °C before further analysis. The

collected fractions were diluted 5000-folds in UPW and sonicated for 15 min in a bath sonicator before SP-ICP-TOF-MS analysis. The operating parameters of the ICP-TOF-MS are provided in **Table S1**.

2.4. Digestion and total metal concentration analysis

A mixture of HNO_3 and HCL, instead of hydrofluoric acid, were used to digest the nanoplastics which have been shown to efficiently digest various types of plastics/polymers including PP, PE< LDPE, HDPE, PS, and PET [55]. Although the HNO_3 and HCL mixture is not sufficient to completely dissolve refractory metal particles such as Ti and Zr, several studies demonstrated the accuracy of measuring these element concentrations using ICP-MS without HF digestion [56, 57]. Approximately 50 mg of the NPO were digested using 4 mL of distilled HNO_3 and 1 mL of distilled HCl (Fisher Chemical, Fair Lan, NJ, USA) in a microwave system (Multiwave Pro, Anton Paar, Ashland, VA, USA). The digestion sequence consists of two steps: a 20-minute power ramp up to 1400W and a 60 min power hold. After cooling, the digestates were diluted in 5 mL 1% HNO_3 and transferred into acid-washed 15 mL centrifuge tubes (Fisher Scientific, Mexico). The samples were bath sonicated (Branson, Model 2800, 40kHz, Danbury, CT, USA) for 15 min and centrifuged at 3100 g (Eppendorf, 5810R, Germany) for 5 min to remove any undigested minerals and prevent clogging the ICP-TOF-MS sample introduction system with large particles. The top 8 mL supernatants were collected for metal analysis using ICP-TOF-MS. Due to the high metal concentrations in the NPO, the digestate supernatants were further diluted 10 folds using 1% HNO_3 before ICP-TOF-MS analysis. All samples were sonicated for 15 min in a bath sonicator before and after dilution. Metal concentration analysis was performed using an ICP-TOF-MS (TOFWERK, Thun, Switzerland). Samples were introduced into the ICP with a 2DX autosampler (Element Scientific, Omaha, United States) and a MicroMist U-series Nebulizer (Thermo scientific, USA) connected via a Quartz Cyclonic Spray Chamber (Meinhard, USA) to the injector of the ICP torch. Additional instrument parameters are provided in Table S1.

2.5. Multi-element single particle analysis

Single-particle analysis of the real-life model nanoplastics (NPO and NPP) and the natural nanoparticles (NPP) were performed using an ICP-TOF-MS (TOFWERK, Thun, Switzerland) to determine all isotopes within individual particles.[58] Element specific instrument sensitivities were measured with a series of multi-element solutions prepared from a mixed multi-element ICP certified reference standard (0, 1, 2, 5, and 10 μgL^{-1} multi-element standard, diluted in 1% HNO_3, BDH Chemicals, Radnor, PA, USA). The transport efficiency was calculated using the known size approach [59] using both Au nanoparticles with a certified particle size of 60 nm (NIST RM8013 Au, Gaithersburg, MD, USA) prepared in UPW and Au ionic standard solutions (0, 1, 2, 5, and 10 μgL^{-1}, diluted in 1% HCl, BDH Chemicals, West Chester, PA, USA). Using a standard tuning solution, the ICP-TOF-MS mass spectra were calibrated based on $^{18}H_2O^+$, $^{59}Co^+$, $^{115}In^+$, $^{140}Ce^+$, and $^{238}U^+$ target isotopes in TofDaq Viewer (Version 2.9, TOFWERK). Dissolved calibration standards were prepared from a mixed multi-element ICP certified reference standard (0, 1, 2, 5, and 10 $\mu g \cdot L^{-1}$, diluted in 1% HNO_3, BDH Chemicals, Radnor, PA, USA) to determine the elemental specific mass responses of particles. A 4.5% H_2/He gas mixture was used as collision gas to eliminate/minimize interferences and was optimized for $^{56}Fe^+$ and $^{28}Si^+$ signals.

All samples were diluted with UPW before analysis to avoid coincidence and eliminate the dissolved background. All samples and UPW blanks were prepared and analyzed in triplicates. The SP-ICP-TOF-MS simultaneously measures all isotopes (mass range of 14-275 amu) at a sampling rate of 33 KHz (30 µs time resolution). However, mass spectra were pre-averaged before readout, resulting in an integration time of 2 ms. Data was acquired for 200 s for each replicate. The data were combined for the three replicates to achieve comprehensive analysis due to limited detection events of certain elements. All data processing – signal thresholding (Poisson algorithm [60]) and split event correction - was performed using Tofpilot (Version 2.9, TOFWERK Ag, Switzerland). The mass and size detection limits assuming pure metal and metal oxide phases are summarized in **Table S2**.

2.6. Agglomerative hierarchical clustering analysis

Detected particle signals were classified into single- and multi-metals nanoplastics (smNPs and mmNPs). The mmNPs were classified into clusters of nanoplastics of similar elemental composition using a two-stage (*e.g.,* intra- and inter-sample) agglomerative hierarchical clustering as performed elsewhere [52, 61, 62]. This process identifies clusters/groups of nanoplastics of similar elemental composition and their mean elemental composition. Briefly, intra-sample clustering was performed on all metal and metalloid masses in each mmNP to generate clusters that best account for variance in mmNP elemental composition in each sample. The dissimilarity matrix was constructed by calculating the pairwise correlation distance between mmNPs based on elemental mass. Then, agglomerative hierarchical clustering was performed using the average correlation distance method. This step generated a unique cluster dendrogram for each sample, divided into major clusters using a specified correlation distance cutoff. The distance cutoff of 0.5, was determined by visually inspecting the dendrogram and through trial and error to minimize the variance/diversity in mmNP elemental composition in the major clusters. Our previous study demonstrated that expert choice and sensitivity analysis of the average silhouette scores can be equally used identify major mmNP clusters [63]. Then, a cluster representative was determined for each major cluster as the mean of metal masses in individual mmNPs within each cluster, considering all elements that occurred in at least 5 percent of mmNPs within the cluster. Then, inter-sample clustering was performed on the major cluster representatives to group/cluster the similar mmNP major clusters identified in the different samples. This step generated a cluster dendrogram for intra-sample cluster representatives, which was divided into major clusters using a distance cutoff of 0.4, as performed for the intra-sample clusters. The intra-sample clustering was performed using the same agglomerative hierarchical clustering method described above.

The mean intra-sample cluster composition was determined as the mean metal mass fraction in all mmNPs in the cluster and was compared across samples. The mass fraction of a given metal in each mmNP

was determined as the mass of that metal divided by the sum of masses of all metals in that mmNP. Select elemental ratios were determined particle-by-particle for all mmNPs containing the select elements. The number concentration (NP mL^{-1}) of the total, smNPs, mmNPs, and cluster members were determined according to the single-particle theory.[59] Finally, heat maps were generated by comparing the number concentration of nanoplastics in each major cluster among the different samples.

3. Results and discussion

3.1. Polymer characterization of environmental nanoplastics

The NPO exhibits a z-average hydrodynamic (d_{zh}) diameter distribution between 100 and 800 nm with a mode d_{zh} of 220 nm [51]. FT-IR spectra of the NPO display characteristic peaks of polypropylene (PP) at 2950, 1376, 979, and 973, and cm^{-1} and polyethylene (PE) at 2850, 720, and 718 cm^{-1} (**Figure S1**). The full (m/z 50 to 260) PyGCMS pyrograms of the NPO are presented in **Figure S2** and illustrate that nanoplastics 1, 2, and 3 have similar pyrolysates, mainly alkene compounds (**Figure S2a** shows the spectrum of nanoplastics 1). In contrast, the nanoplastics 4 pyrogram displays (**Figure S2b**) a large composition heterogeneity, including the presence of natural organic matter, propylene, and a trace of polyethylene. The large signal in the nanoplastics 4 pyrogram corresponds to carbon dioxide, strongly indicating the presence of natural organic matter in the pyrolysis cup. We focus on polymeric markers (*e.g.,* m/z 55 for Nanoplastics 1, 2, and 3 and m/z 70 for Nanoplastics 4) to identify the different polymers present in the NPO. A series of n-alkene compounds from the nonene (C9) at tR=4.03 min up to 1-pentatriacontene (C35) at t_R=19.7 min was identified in nanoplastics 1 (nanoplastics 2 and 3 display similar pyrograms) (**Figure S3a**). This series of n-alkene could originate from polyethylene polymers [64], other polymers, or natural organic matter [65]. However, the triplet of 1,11-dodecadiene, 1-dodecene, and dodecane at elution times of 6.88, 6.96, and 7.02 min, respectively was also identified in the pyrolysates of nanoplastics 1 (**Figure S3b**). This triplet of pyrolysates categorically indicates the presence of polyethylene polymer in nanoplastics 1, 2,

and 3 [64]. Pyrolysates greater than C20 are attributed to the higher mass of pure plastics deposited in the pyrolysis cup (20-30 mg) compared to those (typically few ng) used to analyze environmental matrices. PyGCMS programs of nanoplastics 4 display a triplet centered on the 1-dodecene and the presence of phenolic compounds, suggesting that nanoplastics 4 contains a mixture of polyethylene and organic matter (**Figure S2b**). A relatively high peak also is identified at elution time of 7.7 min with a major ion of m/z 70. The m/z 70 pyrogram of nanoplastics 4 displays four peaks (C9, C12, C15i, and C15s), corresponding to methyl-alkene ion, a unique polypropylene marker (**Figure S3c**) that does not suffer from interferences by pyrolysates generated from natural organic matter [66].

3.2. Metal concentrations and ratios

Substantial concentrations of Al, Fe, Cr, Ni, Mn, Co, Zr, Sn, Sb, and Pb were detected in the NPP (**Figure 1a**). Aluminum and Fe exhibited the highest concentrations, accounting for 37 to 86% and 2 to 46% of all detected metals and metalloids in the nanoplastics. Chromium, Ni, Mn, Sb, Zr, and Sn accounted for 4 to 6.3%, 1.2 to 2.6%, 0.3 to 1.5%, 0 to 4.9%, 0.1 to 1.6% and 0 to 0.7% of all detected metals and metalloids in the nanoplastics. Pb was detected in PSF and Co in PETEB and PSF, accounting for 1.3% and 0.1% of all detected metals and metalloids in the nanoplastics, respectively. Similarly, substantial concentrations of metals and metalloids were detected in the NPO. Silicon exhibited the highest concentration in all these nanoplastics, accounting for 49 to 69% of the sum of all metals and metalloids (**Figure 1b**). Aluminum, Sr, Ti, Fe, and Ba also occurred at high concentrations, accounting for 8 to 12%, 5 to 11%, 4 to 6%, 3 to 4.1%, and 0.5 to 5.2% of metals and metalloids, respectively. Copper, Pb, Zn, Cd, and Cr accounted for 0.1 to 5% of the detected metals and metalloids. All other elements occurred at much lower concentrations, accounting for < 0.1 % of metals and metalloids. Rare earth elements displayed the lowest concentrations among all the metals and metalloids, accounting for < 0.01% each.

Metals are widely used in plastics as additives for pigments, fillers, stabilizers, catalysts, biocides, antimicrobial agents, lubricants, and flame retardants [67, 68]. Silicon and Al are used mainly as fillers. Commonly used fillers in plastics include SiO_2, $CaCO_3$, $BaSO_4$, TiO_2, clays, talc ($MgSi_4O_{10}(OH)_2$), and kaolinite ($Al_2Si_2O_5(OH)$)[30, 31]. Titanium in TiO_2 is used as a white pigment; Cu in the form of $BaCuSi_2O_6$, and $2CuCO_3.Cu(OH)_2$ is used in the blue pigment; Cu, Cd, and Cr are used as green pigments such as the phthalocyanine green (Cu-organic complex), $CuCH_3COO)_2.H_2O$, $CuCO_3.Cu(OH)_2$., $Cr_2O_3.2H_2O$, and a mix of CdS and Cr_2O_3; Pb and Ba are used as yellow pigments such as $Pb_3(SbO_4)_2$, $PbCrO_4$, or Pb_2SnO_4 and $BaCrO_4$. Lead and Ba are also used in plastic formulations as heat stabilizers, antioxidants, UV stabilizers (Pb), and fillers (Ba). Antimony in Sb_2O_3 and Zn are used in plastics as flame retardants. Metals in plastics also can be sorbed from the environment.

The bulk ratios of Ti/Nb, Si/Al, Cr/Fe, and Ni/Fe in the NPO are presented in **Figure 2**. These elemental ratios are substantially higher than the natural background ratios [69], indicating that these elements (Ti, Si, and Cr) are intentionally added to the plastics as pure elements or composites. As discussed above, these elements are widely used in plastics as additives such as pigments and fillers [67, 68].

While considerable work has been on characterizing metal contamination in plastics, particularly in plastic recycling,[70] little attention has been given to identifying elemental fingerprints in nanoplastics vs. those in NNP. Below we discuss the identification of elemental fingerprints in model real-life nanoplastics (NPP and NPO) using transmission electron microscopy and SP-ICP-TOF-MS and agglomerative hierarchical clustering analysis.

3.3. Microscopy analysis

Microscopic analyses, using TEM-EDX, illustrate that the NPO exhibit irregular shapes and consist of a mixture of carbon rich particles, metal rich particles, and composite carbon-metal particles (**Figure 3**). **Figure 3a** shows an example of particles detected in nanoplastics 3 including carbon, aluminum, titanium,

iron, and silicon rich particles. The carbon rich particles are indicative of fragmented polymeric particles. Silicon, Al, and Fe-rich particles were associated with the polymeric fragment. In contrast, this micrograph did not identify Ti-rich particles with the polymer. **Figure 3b-c** shows an example of the particles detected in nanoplastics 2 and illustrates carbon and titanium rich particles that were associated. The titanium-bearing particles were 180-260 nm in size, typical of TiO_2 pigments used in the production of plastics. These metallic particles (*e.g.,* Al, Si, Ti, and Fe) are used in relatively high concentrations in plastics and therefore can be identified by TEM-EDX analysis. However, other metallic particles are used in plastics in much lower concentrations. They therefore are very unlikely to be detected by TEM-EDX measurements due to their rare occurrence compared to polymeric and the more dominant metal and metalloids-bearing particles. Additionally, metals and metalloids could be sorbed on the surfaces of plastics from the surrounding environment, which might be present in much lower concentrations than the metal additives, rendering their detection by TEM rather difficult. Thus below, we further discuss the characterization of the metallic signatures of the model real-life nanoplastics based on SP-ICP-TOF-MS analysis.

3.4. Metallic fingerprint in nanoplastics generated from plastic products

At the single-particle level, metals and metalloids were detected in all the model real-life nanoplastics as single particles. Similar to our previous study [52], all elements - Si and Fe more frequently than other elements due to interferences - were detected as single particles in the procedural blanks at low concentrations . Most of the detected particles in the procedural blanks were smNPs. In contrast, mmNPs were rarely detected in the procedural blanks, suggesting that all mmNPs in nanoplastic samples are actual particles [52]. The number concentration (particles g^{-1} **Figure 4a**) of metal and metalloid-bearing particles was higher in the NNP than in the nanoplastics, except for Cd in all samples and Sb in nanoplastics 1. Additionally, REEs (in particular La, Ce, Pr, and Nd), Hf, and Th occurred at much lower concentrations

(*e.g.,* 12 to 48 folds) in the nanoplastics compared to the NNPs, in agreement with the total metal concentrations discussed above.

The within-sample relative abundance of the detected metallic particles in the nanoplastics and NNPs is presented in **Figure 4b**. Iron, Ti, Pb, Si, Al, Cr, Cu, Zn, and Cd were the most frequently detected elements in nanoplastics. Antimony represented a significant fraction (approximately 5% of all detected elemental signatures) of the detected particles in nanoplastics 1. Antimony is used as a pigment, catalyst, and flame retardant in plastics [68, 71]. Cadmium represented a high proportion of elements detected in NPO (1 to 20%) compared to NPP (<0.04%) and to NNP (< 0.01%), suggesting that Cd metals could have sorbed to the surfaces of ocean plastic fragments from the surrounding environment [72]. Rare earth elements Mo, Sn, Ta, and Th were rarely detected in the nanoplastics and represented a small fraction (<1 % each) of all metal and metalloid-bearing particles detected in plastics. Among the NPP, the LDPEB was particularly rich with Ti-bearing particles, accounting for 55% of all detected metal particles. TiO_2 is the most widely used white pigment in the polymer industry [73]. The PPS and PETEB NPP were rich in Fe, Pb, Cr, and Si-containing particles. The relative abundance of Ti, Al, Cu, Zn, Cd, Nb, and W was higher in NPO than in NPP. This might be attributed to the sorption/attachment of these elements/particles on the surfaces of plastics from the natural environment [72].

The mmNPs were clustered into 30 clusters (**Figure S4a**), including Al, Si, Fe, Ti, Ba, Cr, Pb, Ni, Zn, Sn, Cd, Cu, and Mn-bearing NM clusters. A distance cutoff of 0.5 was selected to group these clusters into major clusters while preserving the identity of most of the clusters. Consequently, 5 to 18 major mmNP clusters were identified in each sample (**Figure S4a**). Inter-sample clustering generated 20 clusters using a distance cut-off of 0.4 (**Figure S4b**). A cutoff of 0.4 was selected to avoid grouping clusters of different elemental compositions into major clusters. The elemental composition (mean mass fraction of metals) of all clusters with at least twenty mmNP members in any sample is presented in **Figure 5,** and those with fewer members in **Figure S5**. Typically, the composition of each cluster is dominated by one metal and

contains minor or trace concentrations of other metals. Four clusters accounted for > 99% of all mmNPs for the NPP, including FeCrTi, TiFeAl, AlFeCu, and SiAlFe clusters (**Figure 5**). These four clusters accounted for > 81% of mmNPs in the NPO. Eleven clusters were necessary to account for > 99% of all mmNPs in the NPO, which includes, in addition to the four clusters identified in the NPP, CdPbCu, CuPbZn, CrPbCo, PbCrTh, ZnFePb, SbPbSn, and BaPbCe. Despite the different filter size cutoff used to separate NPP (< 0.45 μ) and NPO (< 1.2 μm), mmNM with similar elemental compositions (*e.g.,* FeCrTi, TiFeAl, AlFeCu, and SiAlFe) were identified in both types of nanoplastics, indicating that the filtration process does not alter the mmNM elemental composition of the nanoplastics. The different mmNM clusters identified in NPO compared to NPO are attributed to metal sorption from the natural environment. Furthermore, two other clusters, CeLaNd, and ZrPbTh, were abundant in the soil samples accounting for 0.4 to 5.5 and 0.1 to 3.4 of all mmNPs in the soil samples but occurred at very low frequency in the nanoplastics. Clusters identified in NPP and NPO exhibited different elemental fingerprints than those identified in the NNP as discussed below.

Al-rich cluster. All plastic particles detected an Al-rich cluster, representing 2 to 32% of all mmNPs. The MmNPs exhibited higher Al and Pb mass fractions and lower Fe mass fractions than those in NNPs (**Figure 5a**). Copper, Zn, Cd, and Pb were detected more frequently in the NPO than in the NNP and were not detected in the NPP, suggesting they might have been acquired from the surrounding environment. Consequently, the Al/Fe and Al/Cd were higher in nanoplastics than NNP. In contrast, Al/Cu and Al/Pb were lower in the nanoplastic than in NNP, indicating the enrichment of nanoplastics with Cu and Pb compared to NNP.

Fe-rich cluster. Fe-rich cluster was detected in all nanoplastics, representing 13 to 67% of all mmNPs. Iron represented 68 to 85% of the particle masses within this cluster (**Figure 5b**). The mass fraction of Cr and Co was higher in the NPP than in the NPO. Ni and Cu mass fractions were higher in NPO than in NPP in NNP. Cd was detected in the NPO only, suggesting that Cd might be acquired from the environment.

Ti-rich cluster. Ti-rich cluster was detected in all plastic particles, representing 1 to 40% of all mmNPs. Titanium accounted for 77 to 92% of particle masses within this cluster (**Figure 5c**). Iron accounted for 1 to 15% of the particle mass and was highest in NNP than in NPP in NPO. Zinc accounted for 1 to 6% of the particles mass and was highest in the NPP than NPO than NNP. Copper and Cd accounted for 0 to 2% and 0 to 1% particle masses in the NPO and were either not detected or present at a negligible concentration in NPP and NNP.

Si-rich cluster. Si-rich cluster was detected in all nanoplastics and represented 5 to 57% of all mmNPs. Si accounted for 77 to 98% of the particles' masses (**Figure 5d**). Al and Fe accounted for 1 to 14% and 0 to 4% of the particle masses and were higher in NNP than in the NPO than in the NPP. Titanium accounted for 1 to 5% of the particle masses and was higher in the NPO than in the NNP than in NPP. Copper, Zn, and Cd were detected only in the NPO, suggesting they might be acquired from the surrounding environment. Lead was detected in most nanoplastics, suggesting it might have originated from plastic additives and/or the surrounding environment.

Cd-rich cluster. Cd-rich cluster was detected in the NPO only (**Figure 5e**) and represented 1 to 9.7% of all mmNPs. Cadmium accounted for 68 to 73% of particle masses, followed by Pb which accounted for 7 to 27% of the particle masses, Cu which accounted for 1 to 15% of the particle masses, Al, Ti, Fe, Zn, and Ba which accounted for <7%, <4%, <3%, <2%, and <2% of particles masses, respectively. This cluster's occurrence in the NPO suggests that these elements might have been sorbed on the plastics from the natural environment [72].

Cu-rich cluster. Cu-rich cluster was detected in the NPO and the Varina soil only (**Figure 5f**) and represented 1.2 to 7.1% of all mmNPs and < 0.1% of all NNP in the Varina soil. Copper accounted for 59 to 75% of particle masses, Pb, Zn, Cd, Ni, Mn Cr, Mo, Fe, and Al accounted for <30%, <24%, <17%, <8%, <7%, < 5%, <5%, <2%, and <1% of particles masses, respectively. The occurrence of this cluster mainly in

the NPO suggest that these elements might have been sorbed on the plastics from the natural environment [72].

Cr-rich cluster. Cr-rich cluster was detected all samples (**Figure 5g**), and accounted for higher fraction of mmNPs in the NPO (0 to 5%) than in the NPP (0 to 0.8%) than NNP (< 0.1%). Copper, Pb, Co, Ba, Fe, and Cu accounted for 65 to 79%, <30%, <26%, <21%, <15%, and <6% of particles masses, respectively. Titanium, Zr, Sb, Th, Cd, and Mo accounted for <5% of the particle masses. The higher occurrence of this cluster in nanoplastics suggest that this cluster might be due to using these elements as pigments and fillers in plastics and/or due to sorption from the surrounding environment.

Pb-rich cluster. Pb-rich cluster was detected at higher frequency in the NPO (0.6 to 3.6%) than in the NPP (< 0.8%) than in the NNP (<0.3%). Lead, Th, Cr, La, Ce, Ba, Cd, and Cu accounted for 31 to 69%, <69%, <41%, <32%, <28%, <10%, <7% and <7% of particles masses, respectively (**Figure 5h**). All other elements accounted for <5% of the particle masses. The higher occurrence of this cluster in nanoplastics suggest that this cluster might be due to using these elements as pigments and fillers in plastics and/or due to sorption from the surrounding environment.

Zn-rich cluster. Zn-rich cluster was detected at higher frequency in the NPO (0.6 to 2.9%) than in the NPP (< 0.5) and in the soil samples (<0.2%). Zinc, Fe, Ti, Pb, Mn, and Cu 62 to 94%, <20%, <17%, <15%, <12%, and <10% of particle masses, respectively (**Figure 5i**). All other elements accounted for <5% of the particle masses. The higher occurrence of this cluster in nanoplastics suggests that this cluster might be due to using these elements as pigments and fillers in plastics and due to sorption from the surrounding environment.

Sb-rich cluster. Sb-rich cluster was detected mainly in the environmental nanoplastics and accounted for 0.0 to 5.7% of all mmNPs in these samples. Antimony, Sn, and Pb accounted for 62 to 83%, <38%, and <26% of particle masses, respectively (**Figure 7j**). Titanium and Fe accounted for < 2% of the particle

masses each. The occurrence of this cluster in environmental nanoplastics suggests that this cluster might be to sorption from the surrounding environment.

Ba-rich cluster. Ba-rich cluster was detected at a higher frequency in the soil samples (0.3 to 1%) than in the NPO (0.3 to 0.8%) in the NPP (< 0.3%) than in NNP (<0.3%). Barium, Pb, Ce, La, Nd, Ti, Al, Cu, Fe, and Zn accounted for 44 to 76%, <47%, <24%, <23%, <8%, <7%, <7%, <6%, <6%, <5% and <5% of particles masses, respectively (**Figure 5k**). All other elements accounted for <5% of the particle masses. ***Ce-rich cluster***. Ce-rich cluster was detected mainly in the NNP and accounted for 0.4 to 5.5% of all mmNPs in the soil samples. This cluster occurred sporadically in the nanoplastics, suggesting this cluster originated from natural sources. Cerium, La, Nd, Pr, Pb, Th, Fe, and Ba accounted for <59%, 61%, <64%, <29%, <26%, <9%, <8%, and <7% of particles masses, respectively (**Figure 5l**). ***Zr-rich cluster***. Zr-rich cluster was detected mainly in the soil samples and accounted for 0.1 to 3.4% of all mmNPs in the NNP. This cluster occurred sporadically in the nanoplastics, suggesting this cluster originated from natural sources. Zirconium, Pb, Ti, Al, Ce, Ba, and Th accounted for 64 to 96%, <36%, <12%, <10%, <9%, <8%, and <8% of particles masses, respectively (**Figure 5m**). The higher occurrence of Ba, Ce, and Zr clusters in the soil samples suggests that this cluster might be of natural origin.

Because elemental association occurs in different clusters, we calculated select elemental ratios (*e.g.,* Si/Al, Fe/Cr, and Fe/Ni) in all particles containing these element combinations within each sample (**Figure 6**). The NNP display Si/Al between 0.5 and 6, typical of naturally occurring nanoparticles (**Figure 6a**).[52] All nanoplastics exhibited Si/Al ratios between 0.5 and 100 with a bimodal distribution. The first peak corresponds to those in NNP. The second peak ranges between 10 and 100. The NPP displayed a higher fraction of particles with high Si/Al ratios than those in the NPO. This might be due to the interaction of ocean plastics with naturally occurring particles resulting in the increased relative abundance of naturally occurring particles in the NPO. The higher Si/Al in the nanoplastics relative to the NNP might be attributed to using Si as a plastic filler. Most NNP exhibited Fe/Cr and Fe/Ni between 10 and 200 (**Figure 6d and g**).[52]

The NPP exhibited monomodal Fe/Cr and Fe/Ni distributions, varying between 0.5 and 10 (**Figure 6e and h**). The NPO exhibited bimodal distributions representing a mixture between NNP and nanoplastics (**Figures 6f and i**). The lower Fe/Cr and Fe/Ni in the nanoplastics than in the NNP might be attributed to the co-existence of iron, Cr, Ni, and Fe from independent particles within the same nanoplastics. Despite the different filter size cutoff used to separate NPP (< 0.45 μ) and NPO (< 1.2 μm), the elemental ratios of Si/Al, Fe/Cr, and Fe/Ni are consistent for NPP and NPO, suggesting that the filtration cutoff did not impact the elemental ratio with the two types of nanoplastics.

The number concentration and the relative abundance of the multi-metal-containing nanoplastics and the mmNNPs is presented in **Figure 7**. In most cases, the number concentration of a given cluster is higher in the NNP than in the NPO. However, few clusters, such as CdPbCu and SbPbSn were present in the nanoplastics only (Figure 7a). The within sample relative abundance of FeCrTi and SiAlFe cluster is higher in the NPP than in the NNPs than in the NPO, The within sample relative abundance of TiFeAl are higher in the NPO than in the NNPs than in the NPP.

3.5. Environmental implications

This study illustrated the characteristics of real-life model nanoplastics generated from new plastic products (NPP) and environmentally aged ocean plastic fragments (NPO). These model real-life nanoplastics exhibited irregular shapes, were rich in metals and metalloids, and were depleted in rare earth elements. The relative abundance of metals and metalloids, such as Ti, Al, Cu, Zn, Cd, and W, were higher in the NPO than in the NPP, likely due to sorption/attachment from the surrounding environment. These model real-life nanoplastics are very different from the commercially available synthetic nanoplastics (*e.g.,* polystyrene beads), which are spherical and contain no to little metal concentrations. Therefore, these results illustrate the need to investigate the environmental fate and effects of the more environmentally relevant model real-life nanoplastics than the typically studied synthetic nanoplastics.

This is because the occurrence of metal and metalloids in real-life nanoplastics could alter their environmental behaviors, such as flotation and sedimentation, by altering plastics' density. They also may enhance the toxicity of nanoplastics toward aquatic organisms, which has not been fully addressed yet. Additionally, metals in nanoplastics could alter the global biogeochemical cycles of metals and metalloids [74-76]. For instance, nanoplastic-related metals could dominate metal content in the ocean surface water as nanoplastic tend to float at the ocean surface following aggregation whereas natural nanoparticles tend to settle down following aggregation.

There has been recent interest in synthesizing model metal-doped nanoplastics to track nanoplastics in fate in the environment and following uptake in organisms [26]. However, such nanoplastics are spherical, contain many surfactants, and contain only one metal; therefore, they lack an accurate representation of real-life nanoplastics. In contrast, real-life nanoplastics have a mixture of metals and metalloids used in plastics as pigments and fillers and sorbed on the surfaces of plastics from the natural environment. Additionally, the elemental fingerprints of real-life nanoplastics are different from naturally occurring nanoparticles, opening a window toward using these elemental fingerprints to track nanoplastics in laboratory and mesocosm studies as well as in the natural environment. For instance, metal enrichment in nanoplastics or differences in elemental ratios of nanoparticles compared to natural nanoparticles, could be used to track nanoplastics in nanoplastic uptake, fate, and transport experiments or to identify the occurrence of nanoplastics in a given environmental system.

Acknowledgment

This work was supported by US National Science Foundation (Grants No. 1553909 and 1828055) to Dr. Mohammed Baalousha. This work has been subjected to US Environmental Protection Agency (USEPA), Office of Research and Development administrative and quality assurance review and approved for publication. The findings and conclusions in this paper are those of the authors and do not necessarily

represent the views of the USEPA. Mention of trade names or products does not constitute endorsement or recommendation for use.

1. R. E. Schnurr, V. Alboiu, M. Chaudhary, R. A. Corbett, M. E. Quanz, K. Sankar, H. S. Srain, V. Thavarajah, D. Xanthos and T. R. Walker, Reducing marine pollution from single-use plastics (SUPs): A review, *Marine pollution bulletin*, 2018, **137**, 157-171.
2. D. Xanthos and T. R. Walker, International policies to reduce plastic marine pollution from single-use plastics (plastic bags and microbeads): a review, *Marine pollution bulletin*, 2017, **118**, 17-26.
3. R. Lehner, C. Weder, A. Petri-Fink and B. Rothen-Rutishauser, Emergence of nanoplastic in the environment and possible impact on human health, *Environmental science & technology*, 2019, **53**, 1748-1765.
4. P. Europe, Plastics the facts 2014/2015: an analysis of European plastics production, demand and waste data, *Plastic Europe, Brussels*, 2015.
5. R. Geyer, J. R. Jambeck and K. L. Law, Production, use, and fate of all plastics ever made, *Science advances*, 2017, **3**, e1700782.
6. A. L. Andrady, Microplastics in the marine environment, *Marine pollution bulletin*, 2011, **62**, 1596-1605.
7. J. P. da Costa, P. S. M. Santos, A. C. Duarte and T. Rocha-Santos, (Nano)plastics in the environment – Sources, fates and effects, *Science of The Total Environment*, 2016, **566-567**, 15-26.
8. J. Gigault, A. t. Halle, M. Baudrimont, P.-Y. Pascal, F. Gauffre, T.-L. Phi, H. El Hadri, B. Grassl and S. Reynaud, Current opinion: What is a nanoplastic?, *Environmental Pollution*, 2018, **235**, 1030-1034.
9. A. A. Koelmans, E. Besseling and W. J. Shim, Nanoplastics in the aquatic environment. Critical review, *Marine anthropogenic litter*, 2015, 325-340.
10. N. Brennholt, M. Heß and G. Reifferscheid, in *Freshwater microplastics*, Springer, Cham, 2018, pp. 239-272.
11. R. Dris, H. Imhof, W. Sanchez, J. Gasperi, F. Galgani, B. Tassin and C. Laforsch, Beyond the ocean: contamination of freshwater ecosystems with (micro-) plastic particles, *Environmental chemistry*, 2015, **12**, 539-550.
12. L. Neufeld, F. Stassen, R. Sheppard and T. Gilman, 2016.
13. J. G. Derraik, The pollution of the marine environment by plastic debris: a review, *Marine pollution bulletin*, 2002, **44**, 842-852.
14. S. Abbasi, N. Soltani, B. Keshavarzi, F. Moore, A. Turner and M. Hassanaghaei, Microplastics in different tissues of fish and prawn from the Musa Estuary, Persian Gulf, *Chemosphere*, 2018, **205**, 80-87.
15. J. F. Provencher, J. C. Vermaire, S. Avery-Gomm, B. M. Braune and M. L. Mallory, Garbage in guano? Microplastic debris found in faecal precursors of seabirds known to ingest plastics, *Science of the Total Environment*, 2018, **644**, 1477-1484.
16. R. W. Obbard, S. Sadri, Y. Q. Wong, A. A. Khitun, I. Baker and R. C. Thompson, Global warming releases microplastic legacy frozen in Arctic Sea ice, *Earth's Future*, 2014, **2**, 315-320.
17. O. H. Fred-Ahmadu, O. O. Ayejuyo and N. U. Benson, Microplastics distribution and characterization in epipsammic sediments of tropical Atlantic Ocean, Nigeria, *Regional Studies in Marine Science*, 2020, **38**, 101365.
18. A. Cera, G. Cesarini and M. Scalici, Microplastics in freshwater: what is the news from the world?, *Diversity*, 2020, **12**, 276.

19. R. R. Leads and J. E. Weinstein, Occurrence of tire wear particles and other microplastics within the tributaries of the Charleston Harbor Estuary, South Carolina, USA, *Marine pollution bulletin*, 2019, **145**, 569-582.
20. D. Lithner, I. Nordensvan and G. Dave, Comparative acute toxicity of leachates from plastic products made of polypropylene, polyethylene, PVC, acrylonitrile–butadiene–styrene, and epoxy to Daphnia magna, *Environmental Science and Pollution Research*, 2012, **19**, 1763-1772.
21. P. P. G. e Silva, C. R. Nobre, P. Resaffe, C. D. S. Pereira and F. Gusmão, Leachate from microplastics impairs larval development in brown mussels, *Water research*, 2016, **106**, 364-370.
22. J. Bhagat, L. Zang, N. Nishimura and Y. Shimada, Zebrafish: An emerging model to study microplastic and nanoplastic toxicity, *Science of The Total Environment*, 2020, **728**, 138707.
23. F. Zhang, Z. Wang, S. Wang, H. Fang and D. Wang, Aquatic behavior and toxicity of polystyrene nanoplastic particles with different functional groups: complex roles of pH, dissolved organic carbon and divalent cations, *Chemosphere*, 2019, **228**, 195-203.
24. O. O. Fadare, B. Wan, L.-H. Guo, Y. Xin, W. Qin and Y. Yang, Humic acid alleviates the toxicity of polystyrene nanoplastic particles to Daphnia magna, *Environmental Science: Nano*, 2019, **6**, 1466-1477.
25. M. Heinlaan, K. Kasemets, V. Aruoja, I. Blinova, O. Bondarenko, A. Lukjanova, A. Khosrovyan, I. Kurvet, M. Pullerits and M. Sihtmäe, Hazard evaluation of polystyrene nanoplastic with nine bioassays did not show particle-specific acute toxicity, *Science of the Total Environment*, 2020, **707**, 136073.
26. D. M. Mitrano, A. Beltzung, S. Frehland, M. Schmiedgruber, A. Cingolani and F. Schmidt, Synthesis of metal-doped nanoplastics and their utility to investigate fate and behaviour in complex environmental systems, *Nature nanotechnology*, 2019, **14**, 362-368.
27. M. Schmiedgruber, R. Hufenus and D. M. Mitrano, Mechanistic understanding of microplastic fiber fate and sampling strategies: Synthesis and utility of metal doped polyester fibers, *Water research*, 2019, **155**, 423-430.
28. L. Marigliano, B. Grassl, J. Szpunar, S. Reynaud and J. Jiménez-Lamana, Nanoplastic Labelling with Metal Probes: Analytical Strategies for Their Sensitive Detection and Quantification by ICP Mass Spectrometry, *Molecules*, 2021, **26**, 7093.
29. J. Jiménez-Lamana, L. Marigliano, J. Allouche, B. Grassl, J. Szpunar and S. Reynaud, A Novel Strategy for the Detection and Quantification of Nanoplastics by Single Particle Inductively Coupled Plasma Mass Spectrometry (ICP-MS), *Analytical Chemistry*, 2020, **92**, 11664-11672.
30. A. L. Andrady and N. Rajapakse, in *Hazardous Chemicals Associated with Plastics in the Marine Environment*, Springer, 2016, pp. 1-17.
31. D. Lithner, Å. Larsson and G. Dave, Environmental and health hazard ranking and assessment of plastic polymers based on chemical composition, *Science of the total environment*, 2011, **409**, 3309-3324.
32. J. A. Pitt, J. S. Kozal, N. Jayasundara, A. Massarsky, R. Trevisan, N. Geitner, M. Wiesner, E. D. Levin and R. T. Di Giulio, Uptake, tissue distribution, and toxicity of polystyrene nanoparticles in developing zebrafish (Danio rerio), *Aquatic Toxicology*, 2018, **194**, 185-194.
33. J. N. Hahladakis, C. A. Velis, R. Weber, E. Iacovidou and P. Purnell, An overview of chemical additives present in plastics: Migration, release, fate and environmental impact during their use, disposal and recycling, *Journal of Hazardous Materials*, 2018, **344**, 179-199.
34. T. A. Osswald, E. Baur and N. Rudolph, *Plastics handbook: the resource for plastics engineers*, Carl Hanser Verlag GmbH Co KG, 2019.

35. M. Cherif Lahimer, N. Ayed, J. Horriche and S. Belgaied, Characterization of plastic packaging additives: Food contact, stability and toxicity, *Arabian Journal of Chemistry*, 2017, **10**, S1938-S1954.
36. X. Cheng, H. Shi, C. D. Adams and Y. Ma, Assessment of metal contaminations leaching out from recycling plastic bottles upon treatments, *Environmental Science and Pollution Research*, 2010, **17**, 1323-1330.
37. P. Westerhoff, P. Prapaipong, E. Shock and A. Hillaireau, Antimony leaching from polyethylene terephthalate (PET) plastic used for bottled drinking water, *Water Research*, 2008, **42**, 551-556.
38. M. D. Fernández Severini, N. S. Buzzi, A. D. Forero López, C. V. Colombo, G. L. Chatelain Sartor, G. N. Rimondino and D. M. Truchet, Chemical composition and abundance of microplastics in the muscle of commercial shrimp Pleoticus muelleri at an impacted coastal environment (Southwestern Atlantic), *Marine Pollution Bulletin*, 2020, **161**, 111700.
39. E. Fries, J. H. Dekiff, J. Willmeyer, M.-T. Nuelle, M. Ebert and D. Remy, Identification of polymer types and additives in marine microplastic particles using pyrolysis-GC/MS and scanning electron microscopy, *Environmental science: processes & impacts*, 2013, **15**, 1949-1956.
40. V. Godoy, M. A. Martín-Lara, M. Calero and G. Blázquez, Physical-chemical characterization of microplastics present in some exfoliating products from Spain, *Marine Pollution Bulletin*, 2019, **139**, 91-99.
41. S. Karbalaei, A. Golieskardi, D. U. Watt, M. Boiret, P. Hanachi, T. R. Walker and A. Karami, Analysis and inorganic composition of microplastics in commercial Malaysian fish meals, *Marine Pollution Bulletin*, 2020, **150**, 110687.
42. D. Mozhayeva and C. Engelhard, A critical review of single particle inductively coupled plasma mass spectrometry – A step towards an ideal method for nanomaterial characterization, *Journal of Analytical Atomic Spectrometry*, 2020, **35**, 1740-1783.
43. M. v. d. Au, M. Schwinn, K. Kuhlmeier, C. Büchel and B. Meermann, Development of an automated on-line purification HPLC single cell-ICP-MS approach for fast diatom analysis, *Analytica Chimica Acta*, 2019, **1077**, 87-94.
44. W. Qin, H.-J. Stärk and T. Reemtsma, Ruthenium red: a highly efficient and versatile cell staining agent for single-cell analysis using inductively coupled plasma time-of-flight mass spectrometry, *Analyst*, 2021, **146**, 6753-6759.
45. R. Gonzalez de Vega, S. Goyen, T. E. Lockwood, P. A. Doble, E. F. Camp and D. Clases, Characterisation of microplastics and unicellular algae in seawater by targeting carbon via single particle and single cell ICP-MS, *Analytica Chimica Acta*, 2021, **1174**, 338737.
46. F. Laborda, C. Trujillo and R. Lobinski, Analysis of microplastics in consumer products by single particle-inductively coupled plasma mass spectrometry using the carbon-13 isotope, *Talanta*, 2021, **221**, 121486.
47. S. Harycki and A. Gundlach-Graham, Characterization of a high-sensitivity ICP-TOFMS instrument for microdroplet, nanoparticle, and microplastic analyses, *Journal of Analytical Atomic Spectrometry*, 2023, **38**, 111-120.
48. L. Hendriks and D. M. Mitrano, Direct Measurement of Microplastics by Carbon Detection via Single Particle ICP-TOFMS in Complex Aqueous Suspensions, *Environmental Science & Technology*, 2023, **57**, 7263-7272.
49. E. Bolea-Fernandez, A. Rua-Ibarz, M. Velimirovic, K. Tirez and F. Vanhaecke, Detection of microplastics using inductively coupled plasma-mass spectrometry (ICP-MS) operated in single-event mode, *Journal of Analytical Atomic Spectrometry*, 2020, **35**, 455-460.
50. S. Lee, X. Bi, R. B. Reed, J. F. Ranville, P. Herckes and P. Westerhoff, Nanoparticle Size Detection Limits by Single Particle ICP-MS for 40 Elements, *Environ. Sci. Technol*, 2014, **48**, 10291-10300.

51. F. Blancho, M. Davranche, F. Fumagalli, G. Ceccone and J. Gigault, A reliable procedure to obtain environmentally relevant nanoplastic proxies, *Environmental Science: Nano*, 2021, **8**, 3211-3219.
52. M. Baalousha, J. Wang, M. Erfani and E. Goharian, Elemental fingerprints in natural nanomaterials determined using SP-ICP-TOF-MS and clustering analysis, *Science of The Total Environment*, 2021, **792**, 148426.
53. F. Loosli, D. Berti, Z. Yi and M. Baalousha, Toward a better extraction and stabilization of titanium dioxide engineered nanoparticles in model water, *NanoImpact*, 2018, **11**, 119-127.
54. Z. Tang, L. Wu, Y. Luo and P. Christie, Size fractionation and characterization of nanocolloidal particles in soils, *Environmental geochemistry and health*, 2009, **31**, 1-10.
55. F. Pfeiffer and E. K. Fischer, Various Digestion Protocols Within Microplastic Sample Processing—Evaluating the Resistance of Different Synthetic Polymers and the Efficiency of Biogenic Organic Matter Destruction, *Frontiers in Environmental Science*, 2020, **8**.
56. A. L. Fabricius, L. Duester, B. Meermann and T. A. Ternes, ICP-MS-based characterization of inorganic nanoparticles--sample preparation and off-line fractionation strategies, *Anal Bioanal Chem*, 2014, **406**, 467-479.
57. F. Loosli, J. Wang, M. Sikder, K. Afshinnia and M. Baalousha, Analysis of engineered nanomaterials (Ag, CeO2 and Fe2O3) in spiked surface waters at environmentally relevant particle concentrations, *Science of The Total Environment*, 2020, **715**, 136927.
58. L. Hendriks, A. Gundlach-Graham, B. Hattendorf and D. Günther, Characterization of a new ICP-TOFMS instrument with continuous and discrete introduction of solutions, *Journal of Analytical Atomic Spectrometry*, 2017, **32**, 548-561.
59. H. E. Pace, N. J. Rogers, C. Jarolimek, V. A. Coleman, C. P. Higgins and J. F. Ranville, Determining transport efficiency for the purpose of counting and sizing nanoparticles via single particle inductively coupled plasma mass spectrometry, *Analytical chemistry*, 2011, **83**, 9361-9369.
60. A. Gundlach-Graham, L. Hendriks, K. Mehrabi and D. Günther, Monte Carlo Simulation of Low-Count Signals in Time-of-Flight Mass Spectrometry and Its Application to Single-Particle Detection, *Analytical Chemistry*, 2018, **90**, 11847-11855.
61. J. Wang, M. D. M. Nabi, M. Erfani, E. Goharian and M. Baalousha, Identification and quantification of anthropogenic nanomaterials in urban rain and runoff using single particle-inductively coupled plasma-time of flight-mass spectrometry, *Environmental Science Nano*, 2022, **9**, 714-729.
62. K. Mehrabi, R. Kaegi, D. Günther and A. Gundlach-Graham, Emerging investigator series: automated single-nanoparticle quantification and classification: a holistic study of particles into and out of wastewater treatment plants in Switzerland, *Environmental Science: Nano*, 2021, **8**, 1211.
63. M. Erfani, M. Baalousha and E. Goharian, Unveiling elemental fingerprints: A comparative study of clustering methods for multi-element nanoparticle data, *Science of The Total Environment*, 2023, **905**, 167176.
64. A. Ter Halle, L. Jeanneau, M. Martignac, E. Jardé, B. Pedrono, L. Brach and J. Gigault, Nanoplastic in the North Atlantic Subtropical Gyre, *Environmental Science & Technology*, 2017, **51**, 13689-13697.
65. Y. Picó and D. Barceló, Pyrolysis gas chromatography-mass spectrometry in environmental analysis: Focus on organic matter and microplastics, *TrAC Trends in Analytical Chemistry*, 2020, **130**, 115964.
66. F. Blancho, M. Davranche, H. E. Hadri, B. Grassl and J. Gigault, Nanoplastics Identification in Complex Environmental Matrices: Strategies for Polystyrene and Polypropylene, *Environmental Science & Technology*, 2021, **55**, 8753-8759.

67. A. Turner and M. Filella, Hazardous metal additives in plastics and their environmental impacts, *Environment International*, 2021, **156**, 106622.
68. C. Catrouillet, M. Davranche, I. Khatib, C. Fauny, A. Wahl and J. Gigault, Metals in microplastics: determining which are additive, adsorbed, and bioavailable, *Environmental Science: Processes & Impacts*, 2021, **23**, 553-558.
69. R. Rudnick, S. Gao, H. Holland and K. Turekian, Composition of the continental crust, *The crust*, 2003, **3**, 1-64.
70. M. Huber, A. Welker and B. Helmreich, Critical review of heavy metal pollution of traffic area runoff: Occurrence, influencing factors, and partitioning, *Science of The Total Environment*, 2016, **541**, 895-919.
71. W. Shotyk, M. Krachler and B. Chen, Contamination of Canadian and European bottled waters with antimony from PET containers, *Journal of Environmental Monitoring*, 2006, **8**, 288-292.
72. L. Gao, D. Fu, J. Zhao, W. Wu, Z. Wang, Y. Su and L. Peng, Microplastics aged in various environmental media exhibited strong sorption to heavy metals in seawater, *Marine Pollution Bulletin*, 2021, **169**, 112480.
73. Chemours, *Ti-Pure Titanium dioxide. Polymers, Light and the Science of TiO2.*, 2018.
74. S. Liu, J. Shi, J. Wang, Y. Dai, H. Li, J. Li, X. Liu, X. Chen, Z. Wang and P. Zhang, Interactions between microplastics and heavy metals in aquatic environments: a review, *Frontiers in Microbiology*, 2021, **12**, 730.
75. G. Binda and L. Nizzetto, *Understanding the effects of plastic pollution on the biogeochemical cycle of elements: introducing PLANET project, EGU General Assembly 2022, Vienna, Austria, 23–27 May 2022, EGU22-5567, https://doi.org/10.5194/egusphere-egu22-5567, 2022*, 2022.
76. K. L. Bowman, C. H. Lamborg, A. M. Agather and C. R. Hammerschmidt, The role of plastic debris in the biogeochemical cycle of mercury in Lake Erie and San Francisco Bay, *Marine Pollution Bulletin*, 2021, **171**, 112768.

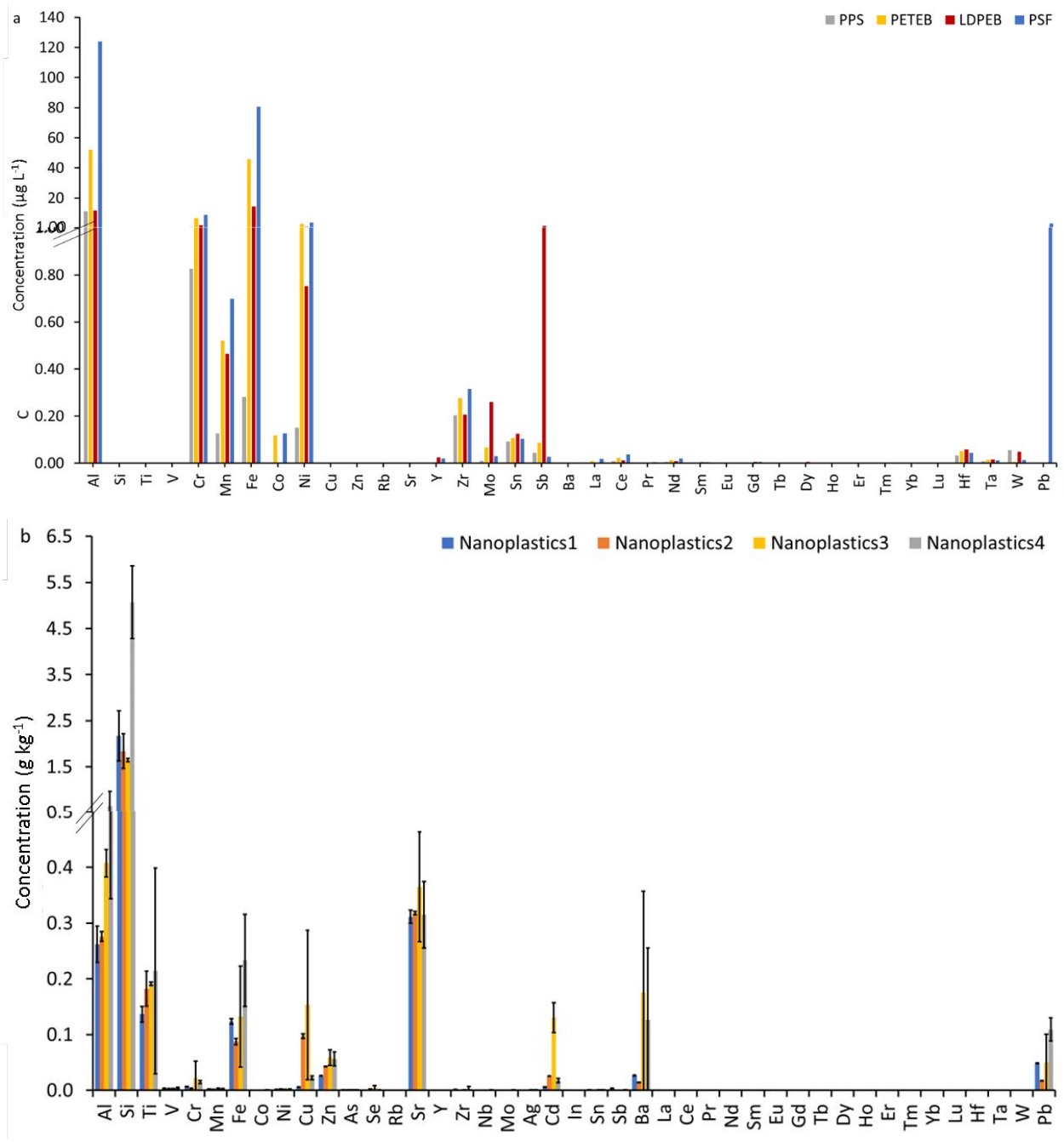

Figure 1. Bulk elemental concentrations in model real life nanoplastics generated from (a) new plastic products (NPP), including polypropylene straw (PPS), polyethylene terephthalate bottle (PETEB), white low density polyethylene bag (LDBEB), and polystyrene foam (PSF) and (b) environmentally aged ocean plastic fragments (NPO), including Nanoplastics 1, 2, 3, and 4. Samples were analyzed using inductively coupled plasma-time of flight-mass spectrometer following microwave assisted acid digestion using a mixture of 4 ml HNO_3 and 1 ml HCl. Data in Figure 1 a represent one replicate whereas those in figure 1b are the mean and standard deviation of three replicates.

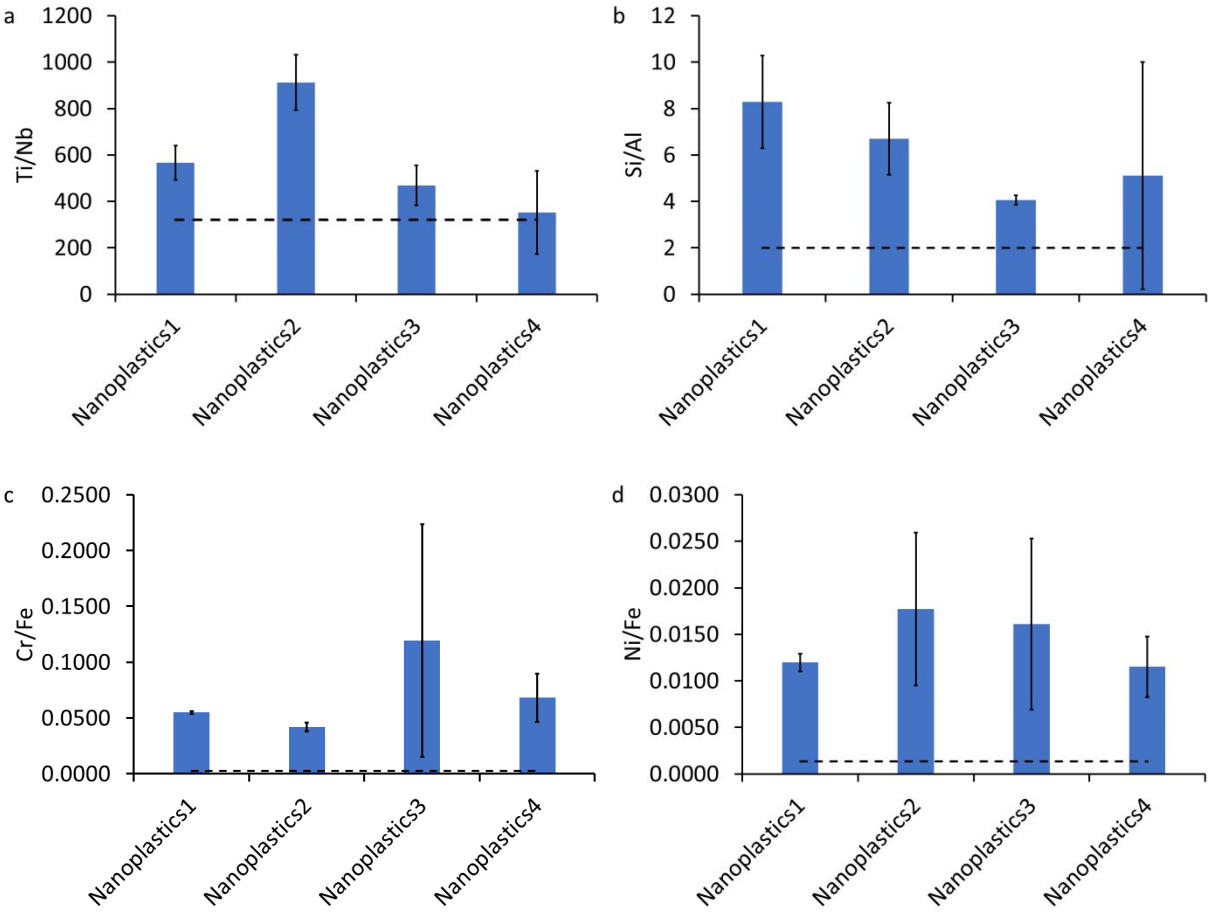

Figure 2. Bulk elemental ratios of (a) Ti/Nb, (b) Si/Al, (c) Cr/Fe, and (d) Ni/Fe in nanoplastics generated from ocean fragments (NPO). The dashed lines represent the natural background ratios. Nanoplastics 1, 2, 3, and 4 refer to the model real-life nanoplastics generated from environmentally aged ocean plastic fragments. Samples were analyzed using inductively coupled plasma-time of flight-mass spectrometer following microwave assisted acid digestion using a mixture of 4 ml HNO_3 and 1 ml HCl.

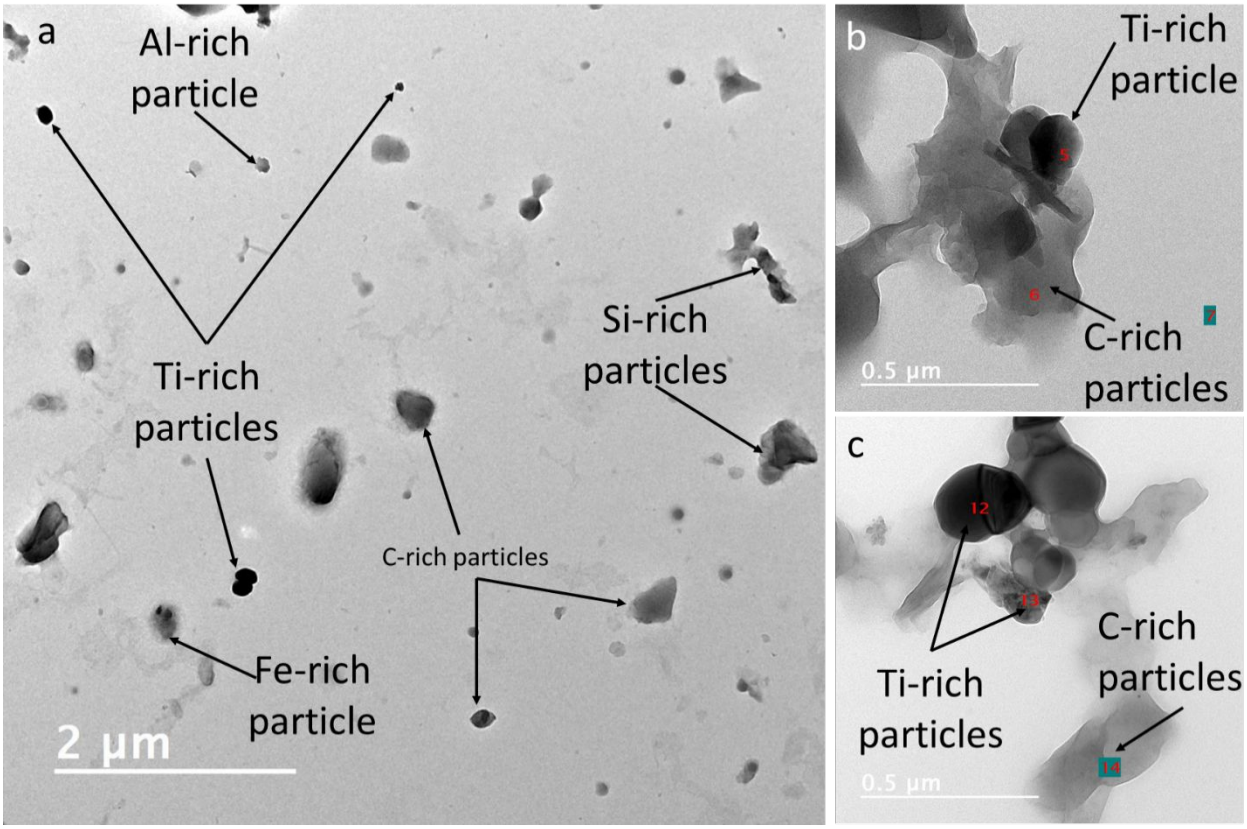

Figure 3. Typical electron microscopy micrographs of the model environmental nanoplastics generated from ocean plastic fragments (NPO): (a) Nanoplastics 3 and (b and c) Nanoplastics 2.

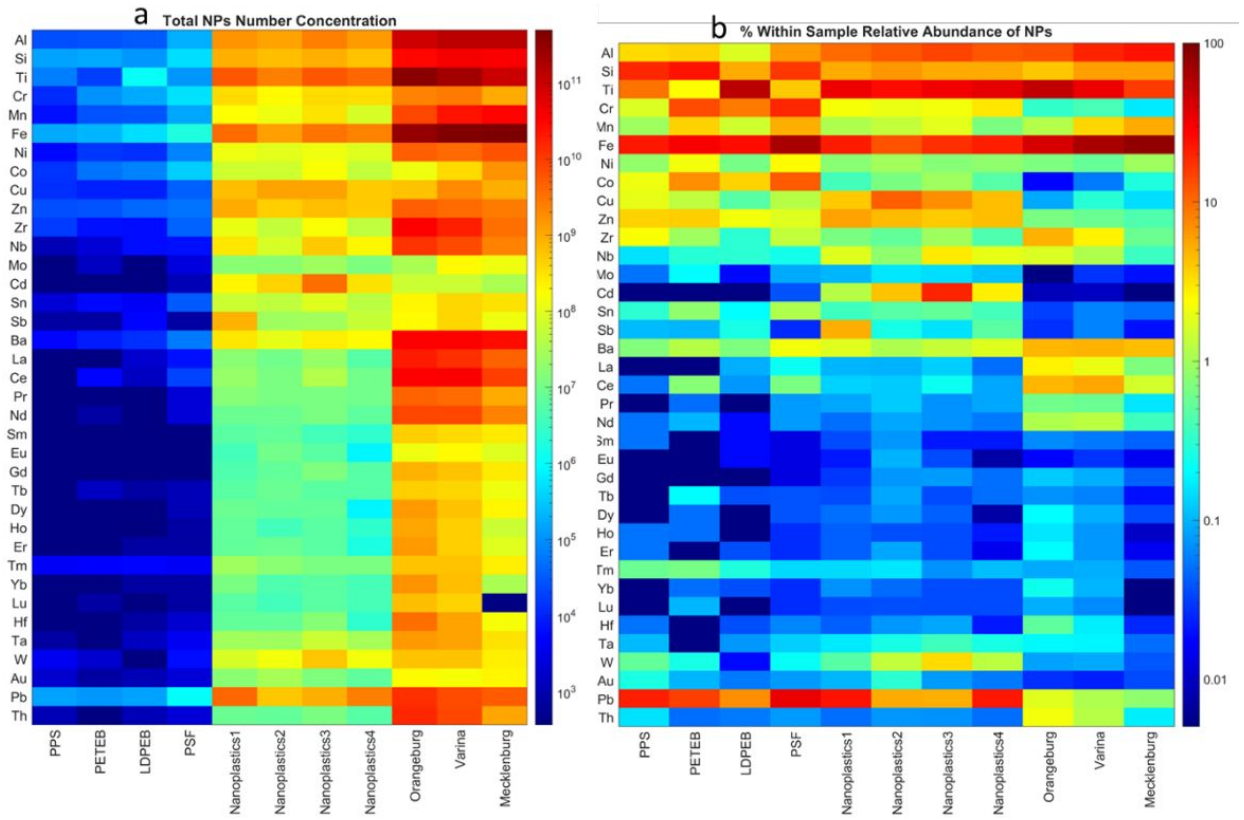

Figure 4. (a) Number concentration and (b) within sample relative abundance of metal-bearing particles in nanoplastics generated from new plastic products (NPP, particle per mL), nanoplastics generated from ocean plastic fragments (NPO, particle per g), and natural nanoparticles (NNP) extracted from three different soils (particle per g). The within sample relative abundance of metal events in nanoplastics were determined by normalizing the number concentration of each metal by the total number concentration of all metal events in a given sample. PPS, PETEB, LDBEB, and PSF refer to the model real-life nanoplastics generated from consumer products, including polypropylene straw, polyethylene terephthalate bottle, white low density polyethylene bag, and polystyrene foam. Nanoplastics 1, 2, 3, and 4 refer to the model real-life nanoplastics generated from environmentally aged ocean plastic fragments. Orangeburg, Varina, and Mecklenburg refer to the three soil samples.

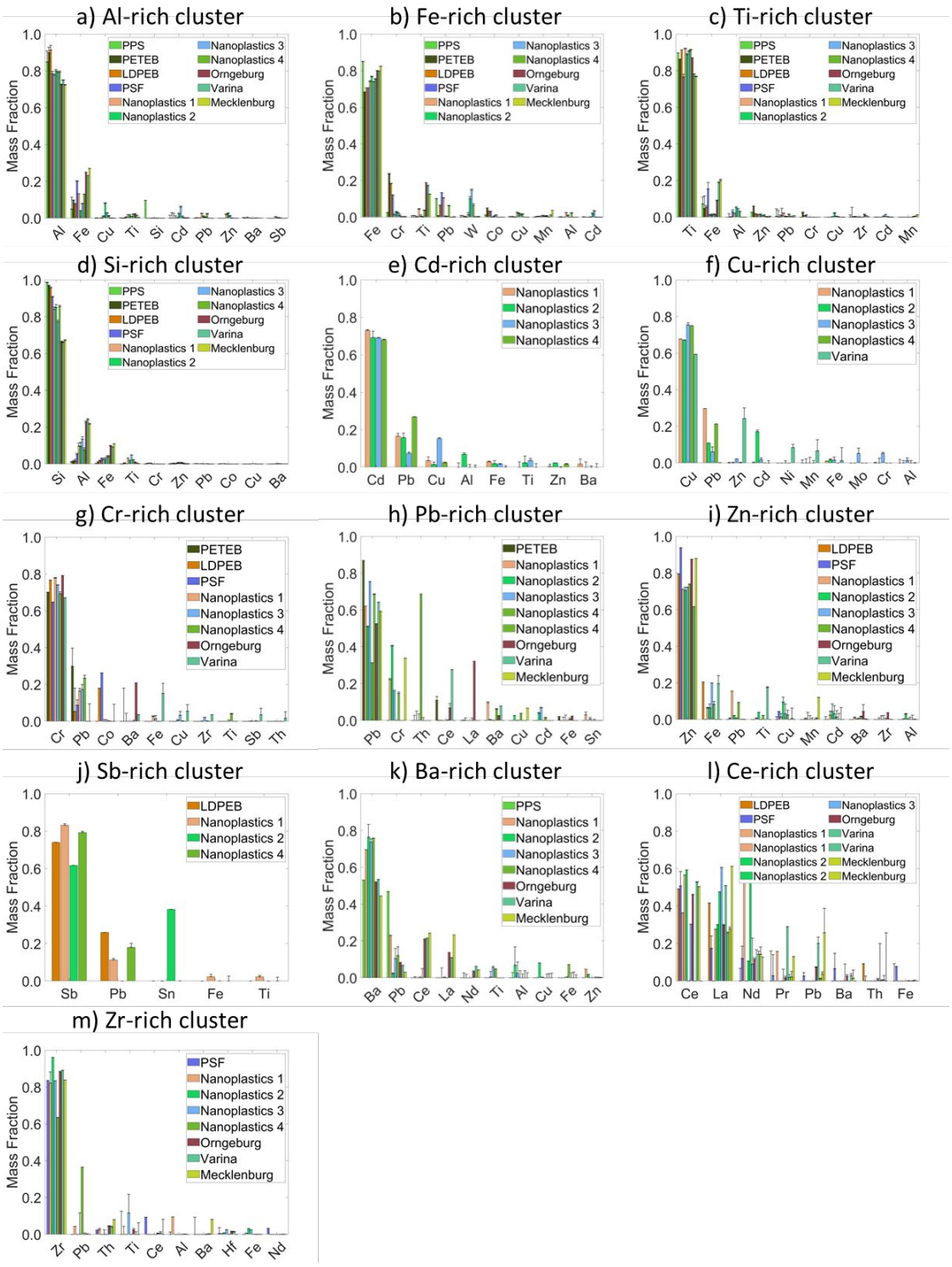

Figure 5. Elemental composition of the multi-metal nanoparticles (mmNPs) clusters identified in nanoplastics generated from fresh plastic products (NPP, PPS, LDPEB, PETEB, and PSF), environmental nanoplastics generated from ocean plastic fragments (NPO, Nanoplastics 1, 2, 3, and 4), and natural nanoparticles (NNPs) extracted from three different soils (Orangeburg, Varina, and Mecklenburg). Only clusters with at least 20 mmNPs detected in at least one sample are presented. First and second stage cutoffs were 0.5 and 0.4, respectively.

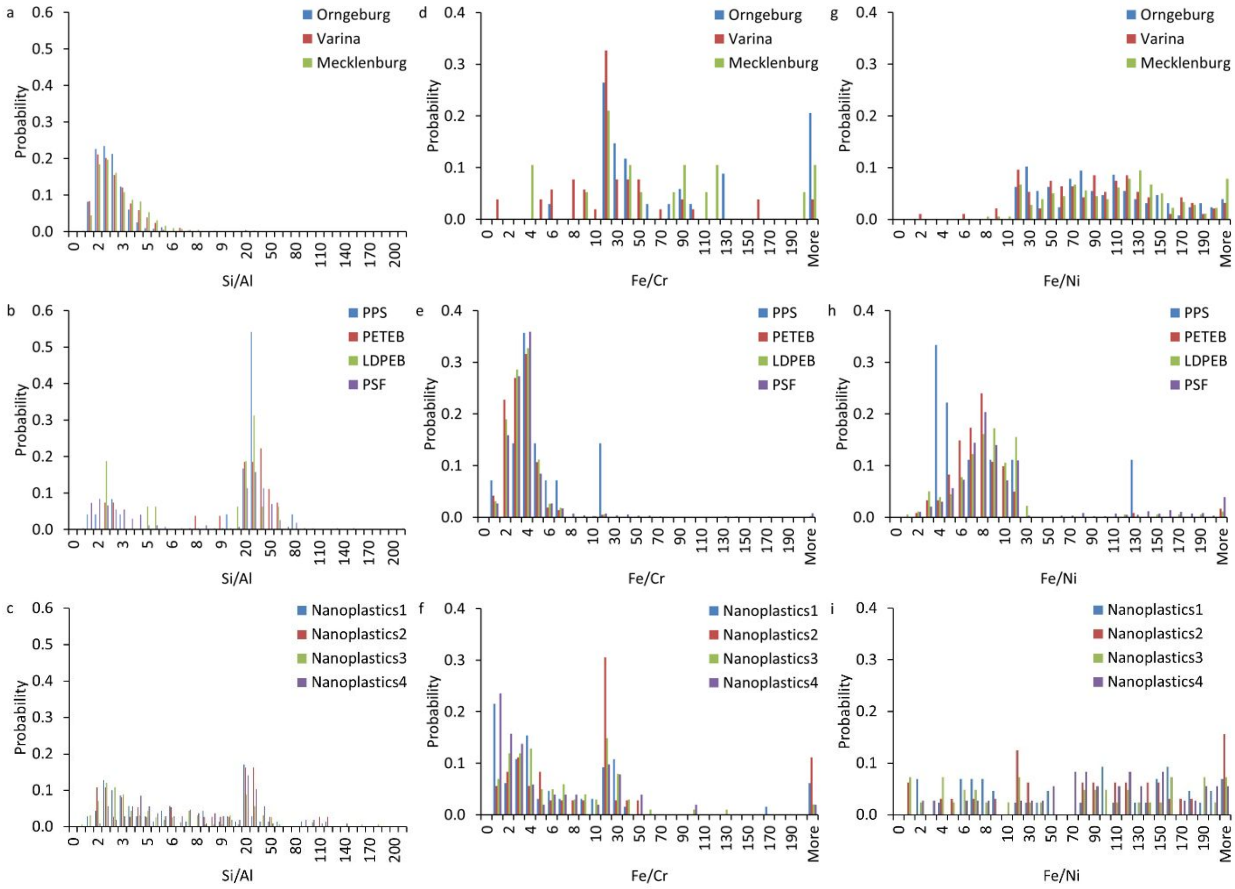

Figure 6. Elemental ratios of (a-c) Si/Al, (d-f) Fe/Cr, and (g-i) Fe/Ni in (a, d, g) soils (NNP), (b, e, h) nanoplastics generated from fresh plastic products (NPP), and (c, f, i) nanoplastics generated from ocean plastic fragments (NPO). First and second stage cutoffs were 0.5 and 0.4, respectively. PPS, PETEB, LDBEB, and PSF refer to the model real-life nanoplastics generated from new plastic products including polypropylene straw, polyethylene terephthalate bottle, white low density polyethylene bag, and polystyrene foam, respectively. Nanoplastics 1, 2, 3, and 4 refer to the model real-life nanoplastics generated from environmentally aged ocean plastic fragments. Orangeburg, Varina, and Mecklenburg refer to the three soil samples.

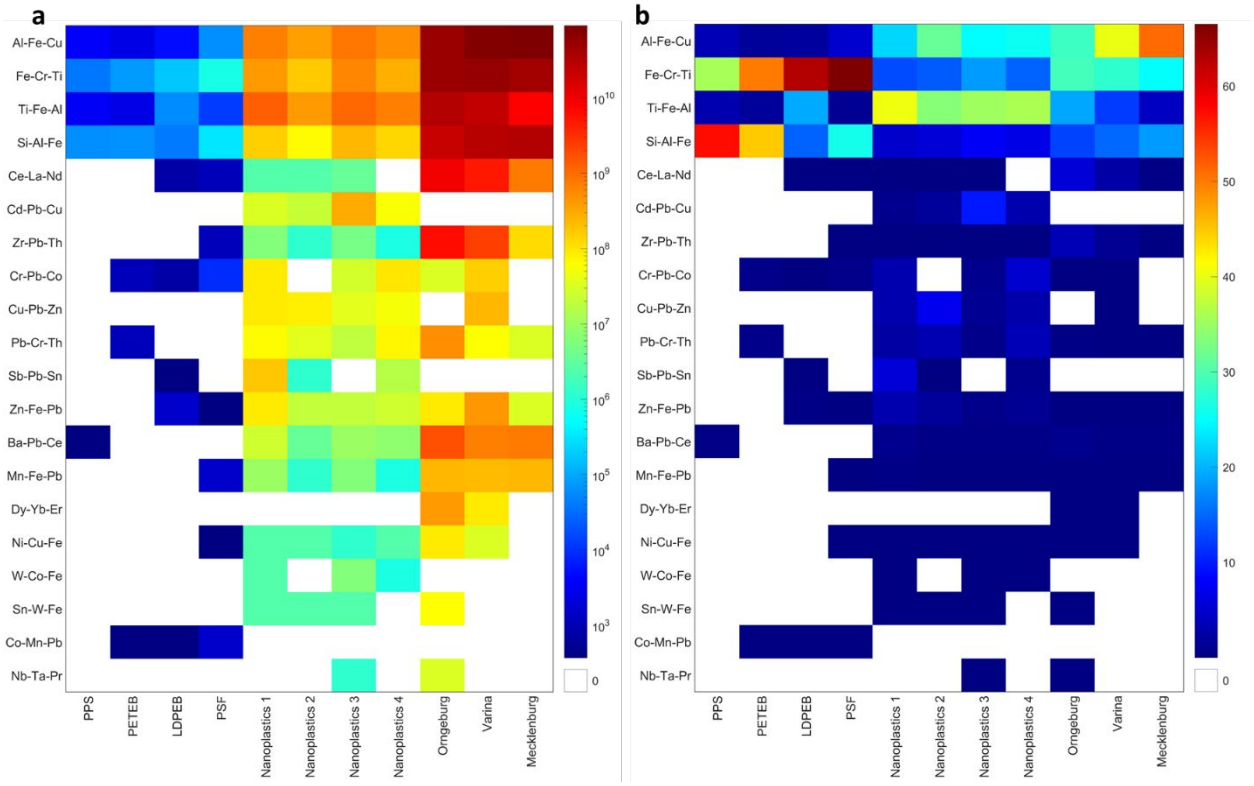

Figure 7. (a) Number concentration and (b) within sample relative abundance of multi-element single particles in the different multi-metal nanoparticles (mmNPs) clusters identified in nanoplastics generated from fresh plastic products (NPP, particle per mL), nanoplastics generated from ocean plastic fragments (NPO, particle per g), and natural nanoparticles (NNP) extracted from three different soils (particle per g). First and second stage cutoffs were 0.5 and 0.4, respectively. Nanoplastics 1, 2, 3, and 4 refer to the model real-life nanoplastics generated from environmentally aged ocean plastic fragments. Orangeburg, Varina, and Mecklenburg refer to the three soil samples.